Journal of Alloys and Compounds 505 (2010) 772–782

Contents lists available at ScienceDirect

Journal of Alloys and Compounds

journal homepage: www.elsevier.com/locate/jallcom

# Role of nano-size reinforcement and milling on the synthesis of nano-crystalline aluminium alloy composites by mechanical alloying

Hafeez Ahamed, V. Senthilkumar*

*Department of Production Engineering, National Institute of Technology, Thiruchirappalli-620015, India*

ARTICLE INFO

*Article history:*
Received 1 April 2010
Received in revised form 21 June 2010
Accepted 22 June 2010
Available online 1 July 2010

*Keywords:*
Nano-crystalline
Al 6063
$Al_2O_3$
$Y_2O_3$
Particle/agglomerate size
Metal matrix composites
Mechanical alloying

ABSTRACT

High-energy wet ball milling was successfully employed to synthesize nano-crystalline Al 6063 alloy powders reinforced with 1.3 vol.%$Al_2O_3$, 1.3 vol.%$Y_2O_3$ and 0.65 vol.%$Al_2O_3$/0.65 vol.%$Y_2O_3$ at nano-size level. In the present study, the crystallite size of the matrix powder particle was affected by the addition of different types of nanoceramic particles separately and in combination keeping total volume percentages of such addition as constant. The nano-composite powders were characterized by SEM, FESEM, HRTEM, XRD, particle size analyzer, EDAX and DTA. Using Williamson–Hall equation, crystallite size and lattice strain of various aluminium composite powders were estimated with broadening of XRD peaks. XRD results showed that the crystallite size of aluminium reached 53 and 37 nm, respectively, after 40 h milling in case of pure Al 6063 and Al 6063/0.65 vol.%$Al_2O_3$/0.65 vol.%$Y_2O_3$ nano-composite powder with uniform particle size distribution. HRTEM observation confirmed the nano-crystalline nature of Al 6063/0.65 vol.%$Al_2O_3$/0.65 vol.%$Y_2O_3$ milled powder.



## 1. Introduction

Interest on powder metallurgy (P/M) aluminium metal matrix composites (MMCs) is increasing, since there is a potential field of applications in aerospace, chemical, transportation, structural and automotive industries. P/M aluminium MMCs have improved strength, high elastic modulus, increased wear resistance, low density, and high stiffness over conventional base alloys [1,2]. Reinforcing aluminium matrix with much smaller particles, submicron or nano-sized range, is one of the key factor in producing high-performance composites, which yields improved mechanical properties. P/M route employing mechanical alloying (MA) is found to be the most economical method for manufacturing aluminium MMCs [3]. Aluminium MMCs are generally manufactured by means of gas-atomized powders, mixing with reinforcement particles by MA process, die compaction, sintering, hot extrusion and heat treatments, to achieve full densification. Final properties of the MMCs depend on matrix and reinforcement particle properties, bonding between reinforcement and matrix, size and distribution of the reinforcement particles into the aluminium matrix. By MA one can avoid the segregation and agglomeration of the reinforcement particles and also, it provides better homogeneous distribution of the reinforcement particles into the aluminium or metallic alloy powders [4,5].

Owing to low density, low melting point, high specific strength and thermal conductivity of aluminium, a wide variety of reinforcement particulates such as SiC, $B_4C$, $Al_2O_3$, AlN, $Si_3N_4$ TiC, $TiO_2$, $TiB_2$ and graphite have been reinforced into it. Among these particulates, SiC, $B_4C$, $Al_2O_3$, $TiB_2$ additions improved the wear behavior of aluminium MMCs. On the other hand, it has been shown that, nano-crystalline matrices strengthened by nano-sized reinforcement are expected to have much better micro-structural stabilities and performance than nano-crystalline materials [6] because of the concurrence of strengthening by both grain-boundary and nanoparticle reinforcements [7–9]. Generally, smaller particles are known to be less susceptible to fracture than long and elongated particles [10]. Previous studies made by the researchers [11–14] show that several composites having a nanometric grain and reinforcing particles of finer/nano size with a more uniform distribution in the matrix can be synthesized by high-energy ball milling process [15]. The high-energy ball milling offers grain size refinement, making the crystals less susceptible to fracture, and hence nanocrystallization process of aluminium MMCs has been the subject of intensive research in recent years.

During high-energy ball milling, whenever two balls collide with each other or when the balls collide with the inner surface of the vial, some amount of starting powder particles are trapped in between them which cause repeated deformation, rewelding and fragmentation of premixed powders resulting in the forma-

* Corresponding author. Tel.: +91 431 250 3519; fax: +91 431 250 0133.
*E-mail addresses:* hafeez_ahamed@rediffmail.com (H. Ahamed), vskumar@nitt.edu (V. Senthilkumar).

0925-8388/$ – see front matter © 2010 Elsevier B.V. All rights reserved.
doi:10.1016/j.jallcom.2010.06.139

tion of fine dispersed hard ceramic reinforcement particles in the grain-refined soft matrix. During the milling operation the two essential processes affect the particle characteristics. First, the cold-welding process leads to an increase in average particle size of the composite, and secondly the fragmentation process causes breaking up of composite particles. Steady-state equilibrium is attained when a balance is achieved between these processes after a certain period of milling. During high-energy ball milling for synthesizing of Al matrix reinforced with nano SiC particles, showed reduced crystallite size significantly rather than that of micron size [16]. Al7075 aluminium alloy doped with graphite nano particles [17] and Al-based nano-composites reinforced with multi-walled carbon nanotubes [18] prepared by MA in a high-energy ball milling showed significant increase in the maximum tensile strength and hardness values. Abdoli et al. showed high strength Al–AlN composite compacts synthesized from high-energy ball milling can be cold compacted and sintered for high densities [19]. For high-energy ball milled powders Nayak et al. showed fully dense Al-based composites could be obtained when cold compaction and sintering is followed by forging [20]. Usually high-energy ball milling is carried out under inert gas, liquid or solid process control agent or in dry air atmosphere. Usage of toluene (sulphur free) as a process control agent in high-energy wet ball milling has negligible amount of iron contamination as reported in the earlier work [21].

The main contribution to the strengthening of MMCs, is not only the grain size refinement and reinforcing particle size, but also the particle addition. Several particle parameters which affect the mechanical properties of MMCs, include the volume fraction ($v_f$), size, shape, and distribution of reinforced particles within the metal matrix. The most influential among these parameters is volume fraction [22]. Earlier studies made by the researchers [23–26] showed that the maximum yield strength, ultimate tensile strength and ductility of nano-sized reinforced matrix composites started decreasing when the volume fraction of nano reinforcement addition exceeds 1.5%.

In this paper, an attempt was made to synthesize Al 6063, Al 6063/1.3 vol.%$Al_2O_3$, Al 6063/1.3 vol.%$Y_2O_3$ and Al 6063/0.65 vol.%$Al_2O_3$/0.65 vol.%$Y_2O_3$ nano composite powders by high-energy ball milling. Reports on enhanced hardness, strength and ductility of MMCs due to the presence of meta-stable, finer precipitation, resistance to high-temperature creep and grain refinement properties provide the importance to the selection of thermally stable nano-sized $Al_2O_3$ and $Y_2O_3$ particulates as reinforcements [27–30]. In the present study, the nano reinforcement of 1.3% volume fraction ($v_f$) is kept constant for all the systems under investigation [24]. The role of hard nano-sized particle reinforcement and milling time on the powder surface morphology, particle shape, size and distribution, crystallite size and lattice strain for different composite powders were investigated. Differential thermal analysis and composition analysis were carried out on the synthesized aluminium composite powders.

**Table 1**
Purity, nominal chemical composition and mesh size used to make 6063 aluminium alloy powder.

| Sl. No. | Name of the elements | Purity % | wt.% | Mesh size |
|---|---|---|---|---|
| 1 | Chromium | 99.9 | 0.1 | −200 to −325 |
| 2 | Copper | 99.7 | 0.1 | −325 |
| 3 | Iron | 99.5 | 0.35 max | −325 |
| 4 | Silicon | 98.5 | 0.2–0.6 | −325 |
| 5 | Zinc | 99.9 | 0.1 | −325 |
| 6 | Magnesium | 99 | 0.45–0.9 | −200 to −325 |
| 7 | Manganese | 99.8 | 0.1 | −200 to −325 |
| 8 | Titanium | 99 | 0.1 | −200 to −325 |
| 9 | Aluminium | 99.7 | Balance | −325 |

## 2. Experimental procedures

### 2.1. Materials

The base material used in the present experimental investigation is Aluminium 6063 (Al 6063), whose nominal chemical composition (wt.%), purity and mesh size of the pure elemental powders supplied by Kemphasol, Mumbai, India is listed in Table 1.

Yttrium oxide ($Y_2O_3$) powder of 99.5% purity with a particulate size range of 25–50 nm, and aluminium oxide ($Al_2O_3$) powder of 99.995% purity with a particulate size range of 40–50 nm supplied by Alfa Aesar, USA, were used as the particulate reinforcements. Volume fraction of 1.3% was used as reinforcement level in the present investigation for the synthesis of all systems of composite mixture.

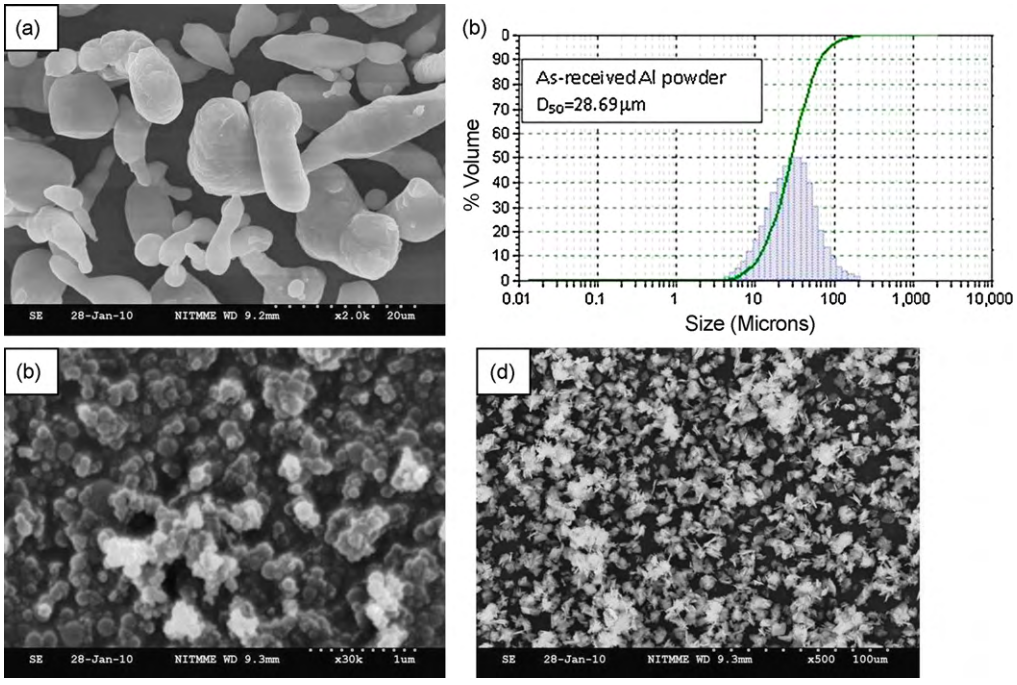


**Fig. 1.** (a) Morphology of as-received aluminium powder (b) Particle size distribution of as-received aluminium powder. (c) Morphology of as-received nano$Al_2O_3$ powder (d) Morphology of as-received nano$Y_2O_3$ powder.

*2.2. Processing*

Al 6063, Al 6063/1.3 vol.%$Al_2O_3$, Al 6063/1.3 vol.%$Y_2O_3$ and Al 6063/0.65 vol.%$Al_2O_3$/0.65 vol.%$Y_2O_3$ nano-composites were synthesized using powder metallurgy technique. The synthesis process involved blending of elemental powders of Al 6063 composition and the reinforcement of nano-sized powders in a two station Insmart Systems, laboratory scale high-energy planetary ball mill at 200 rpm for one and half hours. No ball and process control agent were used during

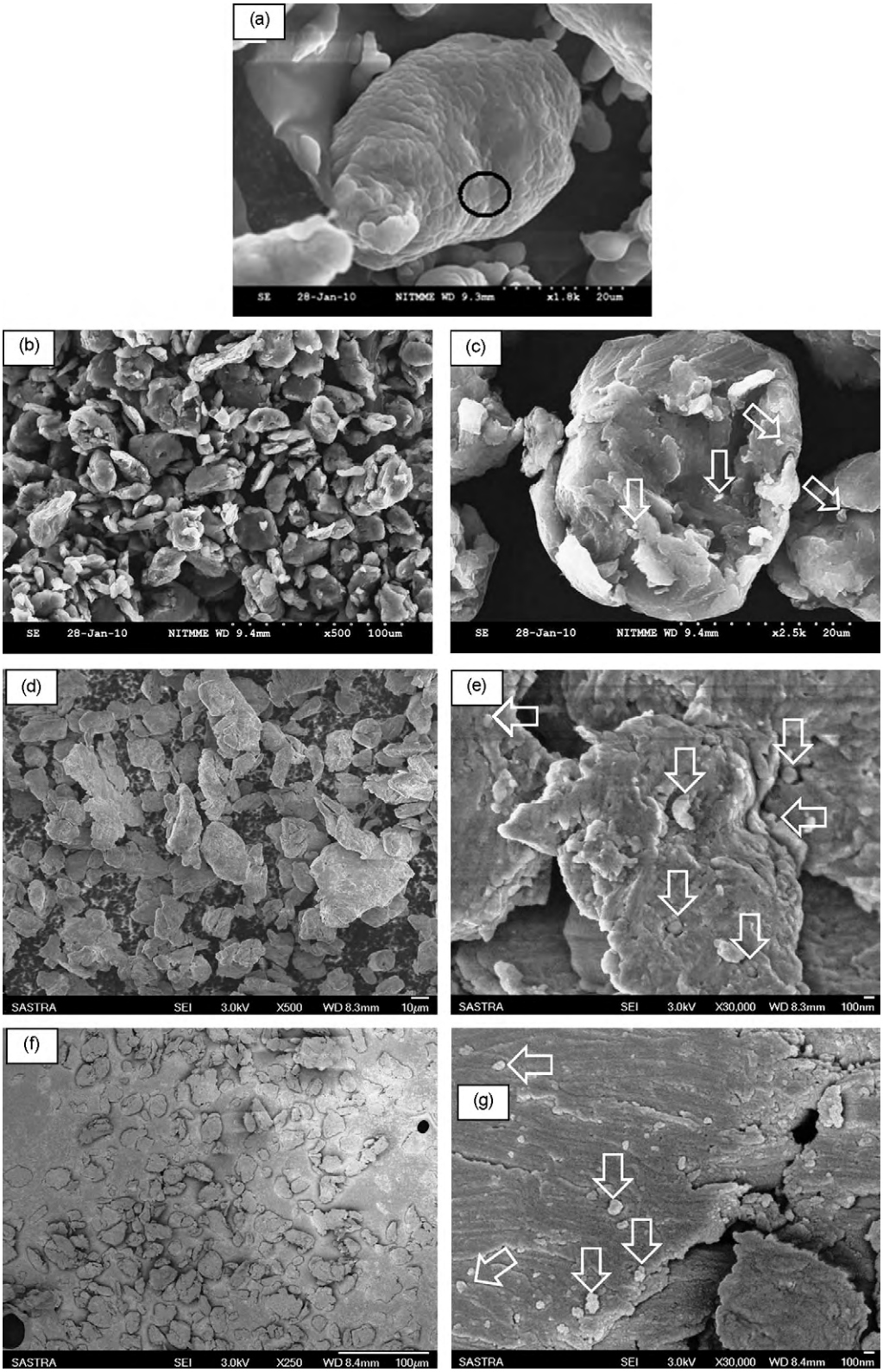


**Fig. 2.** (a) The morphology of as-received single aluminium particle. The morphology of powder after 40 h milling: (b) Al 6063 (c) Magnified view of 'b' (d) Al 6063/1.3$Al_2O_3$ (e) Magnified view of 'd' (f) Al 6063/1.3$Y_2O_3$ (g) Magnified view of 'f' (h) Al 6063/0.65$Al_2O_3$/0.65$Y_2O_3$ (i) Magnified view of 'h'. Arrows indicates examples of nano particles. (j) SEM–EDS micrograph of 40 h milled Al 6063/0.65$Al_2O_3$/0.65$Y_2O_3$ powder showing good interfacial integrity between Al matrix and nano particles. The corresponding EDX spectrum shown as inset verifies the presence of nano particles.

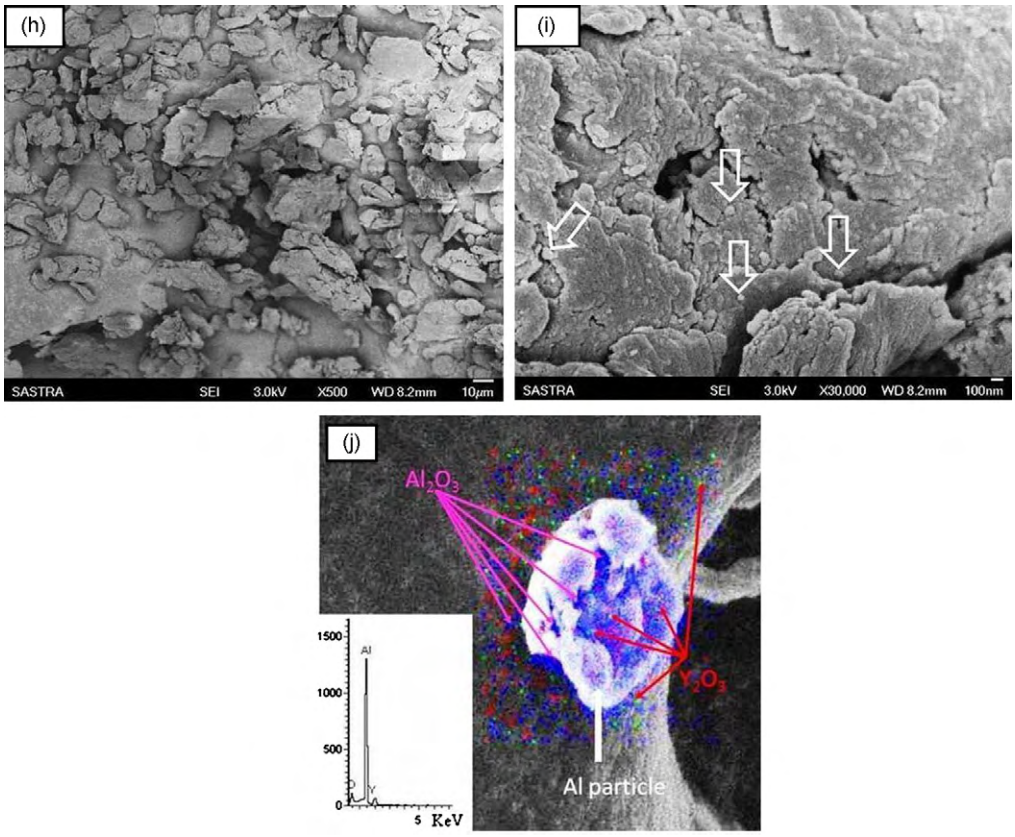


**Fig. 2.** (*Continued*).

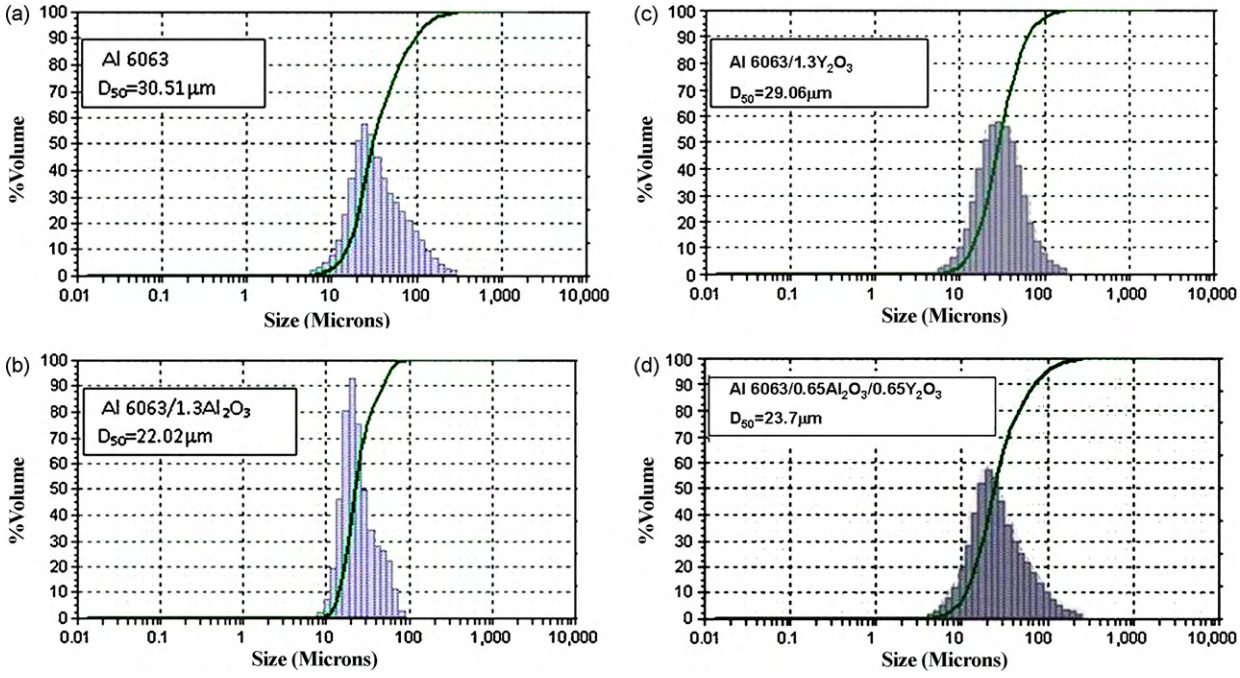


**Fig. 3.** Particle size distributions of nano-crystalline powders (a) Al 6063 (b) Al 6063/1.3$Al_2O_3$ (c) Al 6063/1.3$Y_2O_3$ (d) Al 6063/0.65$Al_2O_3$/0.65$Y_2O_3$ milled powder after 40 h. The highest peak of the column is the equivalent diameter size ($D_{50}$).

**Table 2**
$D_{50}$ and $D_{90}$ values related to the particle size distributions of powders after 40 h of milling.

| Powder | $D_{50}$ (μm) | $D_{90} - D_{10}$ (μm) |
|---|---|---|
| Al | 28.69 | 54.6 |
| Al 6063 | 30.51 | 79.23 |
| Al 6063/1.3$Al_2O_3$ | 22.02 | 33.56 |
| Al 6063/1.3$Y_2O_3$ | 29.06 | 48.52 |
| Al 6063/0.65$Al_2O_3$/1.3$Y_2O_3$ | 23.7 | 58.91 |

the blending process. The blended powder was regarded as the 0 h mechanically milled powder.

The volume fraction $v_f$ of reinforcement is calculated through mass density ($\rho$) of particles and alloy powders ($Al_2O_3$, 3.95–4.1 g/cm$^3$, $Y_2O_3$, 5.01 g/cm$^3$, Al 6063, 2.73 g/cm$^3$) using the following equation,

$$v_f = \frac{(w/\rho_{\text{Particle}})}{(w/\rho_{\text{Particle}}) + ((1-w)/\rho_{\text{Al 6063}})} \quad (1)$$

where $w$ is the weight percentage of the reinforcement particle.

Powder blends were then subjected to high-energy ball milling (Insmart Systems, Hyderabad, India.) with the following parameters: charge ratio: 10:1 (wt.); powder mass: 30 g; mass of balls: 288 g; ball diameter: 16 mm; ball material: hardened stainless steel; no. of balls: 18; plate speed: 150 rpm: vial speed: 300 rpm; vial material: hardened stainless steel; A total of 75 ml of Toluene (PCA) (Sulphur free supplied by Ranbaxy, India) was added in each vial to control the process in order to avoid formation of inter-metallic compounds during milling. The constituent powders were milled continuously for 40 h. The high-energy milling time was the time necessary to complete the mechanical alloying process. The milling process was systematically studied by extracting powder samples for every 10 h to know the grain refinement and micro-structural changes. The ball milling experiments were stopped periodically for every 15 min and then resumed for 15 min, in order to avoid significant temperature rise. Powder samples are designated by Al 6063, Al 6063/1.3$Al_2O_3$, Al 6063/1.3$Y_2O_3$ and Al 6063/0.65$Al_2O_3$/0.65$Y_2O_3$.

### 2.3. Powder characterization

X-ray diffraction analysis was carried out to determine the crystallite size and lattice strain of the milled powder samples on D/MAX Ultima III, XRD machine (Rigaku Corporation, Japan). The samples were exposed continuously to Cu Kα radiation (λ = 1.5406 Å) operated at 40 kV/30 mA and at a scanning speed of 2°/min for a scanning range of 20–100° in steps of 0.02. Williamson and Hall [31] proposed a method of deconvoluting size and strain broadening by looking at the peak width as a function of diffracting angle $2\theta$ and the instrumental corrected broadening, $\beta_{hkl}$, corresponding to the diffraction peak of Al was estimated using the following equation

$$[\beta_{hkl} \cos\theta_{hkl}] = \left[\frac{K\lambda}{t}\right] + [4\ \varepsilon\ \sin\theta_{hkl}] \quad (2)$$

where $K$ is the shape factor (0.9), λ is the X-ray wavelength (1.5406 Å), $\theta_{hkl}$ is the Bragg angle and $t$ is the effective crystallite size normal to the reflecting planes and $\varepsilon$ is the lattice strain. The instrumental corrected broadening, $\beta_{hkl}$, was approximated by a Gaussian fit, as full width at half-maximum (FWHM) which was calculated by using X-ray diffraction Analysis software based on each diffracting angle of $2\theta$. The first four and five Al reflecting planes (1 1 1), (2 0 0), (2 2 0), (3 1 1) and (2 2 2) were used to construct a linear plot of $\beta_{hkl} \cos\theta_{hkl}$ as a function of $4\varepsilon \sin\theta_{hkl}$, the crystallite size $t$ may be estimated from the intersection with the vertical axis [$K\lambda/t$] and the lattice strain $\varepsilon$ from the slope of the line [31].

Lattice parameter at 40 h of milled powder was estimated by constructing the linear plot between the calculated lattice parameter for each Bragg's angle on the $y$-axis and the corresponding value of $\cos^2\theta_{hkl}/\sin\theta_{hkl}$ on the $x$-axis. The actual lattice parameter was estimated from the intercept as explained by Cullity [32].

The morphology of powder particles was investigated by scanning electron microscopy (SEM) using HITACHI S 3000H and field emission scanning electron microscopy (FESEM) using JEOL 6701F scanning electron microscope. JEOL 3010 high-resolution transmission electron microscope (HRTEM) was used for investigating the nano-crystalline nature of the nano-composite powder. Particle size distribution was determined by LASER diffraction (Bluewave, Microtrac), connected to a computer that makes the volume size distribution, $D_{10}$ to $D_{90}$ calculation automatically. For Al 6063 and Al 6063/0.65 vol.%$Al_2O_3$/0.65 vol.%$Y_2O_3$, 40 h milled powder Energy dispersive X-ray analysis (EDAX) was conducted for compositional analysis and differential thermal analysis (DTA) was also conducted to study the powder displacement reactions for which the samples were heated in nitrogen atmosphere up to 800 °C at a rate of 20 °C/min.

## 3. Results and discussion

### 3.1. Effect of reinforcement and milling time on morphology and size of matrix powder

Fig. 1(a)–(d) shows the morphologies of the as-received aluminium alloy powder and reinforcement particles, i.e., nano-sized $Al_2O_3$ and $Y_2O_3$. The aluminium matrix powder particles shown in SEM image of Fig. 1(a) are irregularly shaped with a relatively broader size distribution. The average particle/agglomerate size ($D_{50}$) is 28.69 μm. Particle size distribution of the as-received aluminium alloy matrix powder using laser scattering method is shown in Fig. 1(b). The laser scattering particle size distribution exhibits uniform size distribution of matrix powder. Fig. 1(c) shows the SEM image of nano-sized $Al_2O_3$ particles which are spherical in shape and at this stage, it can be seen that most of the particles are agglomerated or clustered. Fig. 1(d) shows the SEM image of nano-sized $Y_2O_3$ particles, which are clustered or agglomerated and are in polygonal and dendritic shapes.

During high-energy milling, plastic deformation, cold-welding and fracture are predominant factors, in which the deformation leads to a change in particle shape, cold-welding leads to an increase in particle size and fracture leads to decrease in particle size [4]. As a result, composite powder particles with a characteristically layered microstructure were formed. Fig. 2 shows the SEM micrographs of MA powders after 40 h milling and confirms the formation of layered microstructure and homogeneous distribution of nano-sized $Al_2O_3$ and $Y_2O_3$ particles in the soft aluminium matrix. Fig. 2(a) reveals, that the as-received aluminium powder has smooth surfaces with orange skin liked topology, commonly exhibited by gas-atomized powders. The maximum size of the observed internal structures was about 382 nm as encircled in figure. Composite powders milled for 40 h revealed formation of clusters of fine particles and heavily deformed fine internal struc-

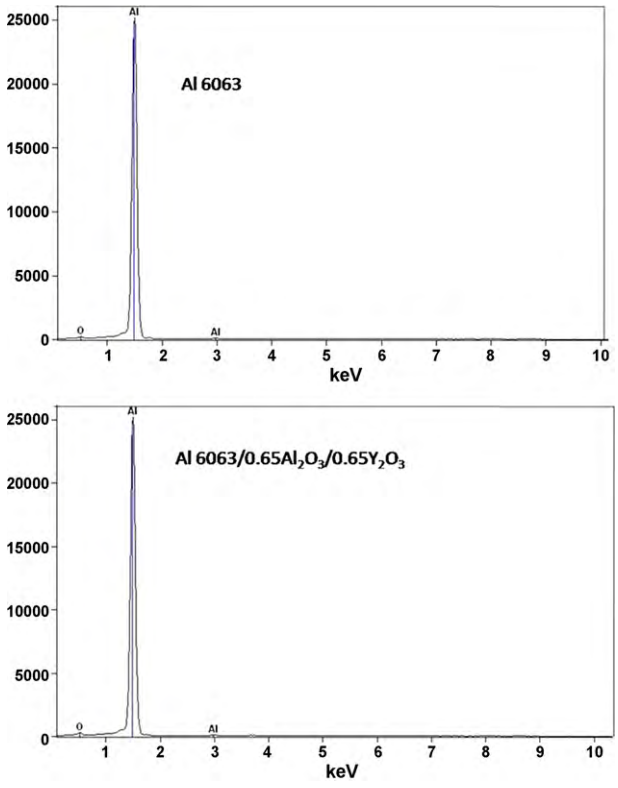


**Fig. 4.** EDX analysis showing the absence of Fe contamination powder milled for 40 h milling: (a) Al 6063 (b) Al 6063/0.65$Al_2O_3$/0.65 $Y_2O_3$.

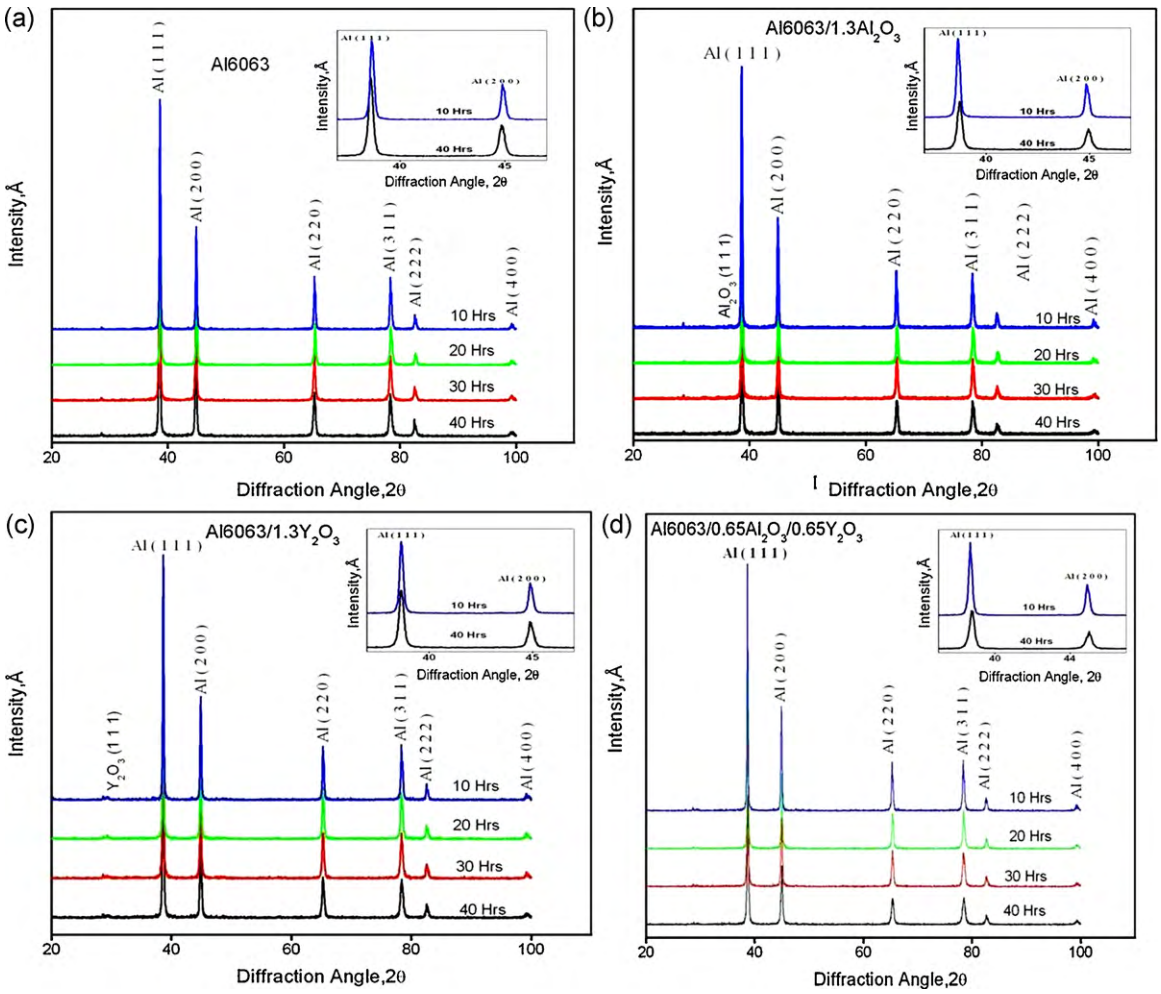


**Fig. 5.** XRD patterns of (a) Al 6063 (b) Al 6063/1.3$Al_2O_3$ (c) Al 6063/1.3$Y_2O_3$ (d) Al 6063/0.65$Al_2O_3$/0.65$Y_2O_3$ composite powder after 10, 20, 30 and 40 h of milling, showing the sharp diffraction peaks of Al getting broadened and reduced in intensity. Inset shows shift in Bragg's angle.

ture less than 53 nm in size (Fig. 2(b)–(i)). This agrees to a great extent with the crystallite size measurements made by XRD analysis, reported in the subsequent Section 3.4.

Fig. 2(b) shows Al 6063 powder morphology after 40 h of MA. The particle shaped almost equiaxed and seen in a spherical form, which is the characteristic of particles at steady-state condition with a refined microstructure and a randomly oriented interfacial grain boundaries which are obtained at this state. It was observed from the Fig. 2(a) and (c) that the average matrix particle/agglomerate sizes are 29 and 31 μm at 0 and 40 h of milling, respectively. Also, the Fig. 2(c) showing the magnified view of Al 6063 powder morphology after 40 h reveals some of other alloying matrix particles which are smeared on the surfaces/completely embedded/dispersed in the soft Al alloy matrix. Arrows in the Fig. 2(c), indicates examples of other alloying matrix particles. A similar behavior was also reported in the MA of PM6061 system [5,26]. The effect of 1.3$Al_2O_3$, 1.3$Y_2O_3$ and 0.65$Al_2O_3$/0.65$Y_2O_3$ reinforcement addition on the morphology of the composite powder during mechanical alloying after 40 h was shown in Fig. 2(b), (d) and (e), respectively. The particles which shaped almost equiaxed with a very fine refined microstructure and randomly oriented interfacial grain boundaries are obtained during milling in all the systems under investigation. It is observed that the average alloy matrix particle/agglomerate sizes are 22, 29 and 24 μm after 40 h for 1.3$Al_2O_3$, 1.3$Y_2O_3$ and 0.65$Al_2O_3$/0.65$Y_2O_3$, respectively. The increased fracturing tendency dominating the soft ductile matrix particle–particle cold-welding in the case of 1.3$Al_2O_3$ reinforcement was observed due to more collision with balls and more support from spherical shaped hard ceramic particles. This resulted in the formation of very fine particles in the case of 1.3$Al_2O_3$ when compared to other systems. The irregular shaped nano-sized 1.3$Y_2O_3$ particles resulted in a larger particle size, when compared with the addition of nano-sized 1.3$Al_2O_3$ particles. The addition of 0.65$Al_2O_3$/0.65$Y_2O_3$ nano particles combination into the Al 6063 blend during milling leads to the reduction in fracture toughness and thus increase the tendency of fracture. Also the presence of hard particles results in increased local deformation of the matrix in the vicinity of the reinforcement particles enhancing the work hardening rate of the matrix. This increased work hardening rate of the alloy may be regarded as another reason for the decreased fracture toughness. Similar results were reported by Khakbiz and Akhlaghi [15] for the Al–$B_4C$ system. Hence it is noteworthy to say that, under identical condition of milling, the addition of nano-sized $Al_2O_3$ and $Y_2O_3$ hard particles separately or in combination into the Al 6063 blend, results in decreased size of the particle/agglomerate confirming the acceleration of the milling process and the formation of equiaxed particles with very fine refined microstructure and randomly oriented grain boundaries which is in good agreement with the earlier work of Razavi-Hesabi et al. [33], this indicates that milling approached to the equilibrium condition. Arrows in Fig. 2(e), (g) and (i), indicate examples of $Al_2O_3$ and $Y_2O_3$ reinforcement particles smeared/engaged/entrapped on the surfaces of soft aluminium matrix particles. Fig. 2(j) represents the SEM–EDS micrograph of Al 6063/0.65$Al_2O_3$/0.65$Y_2O_3$ powder milled for 40 h,

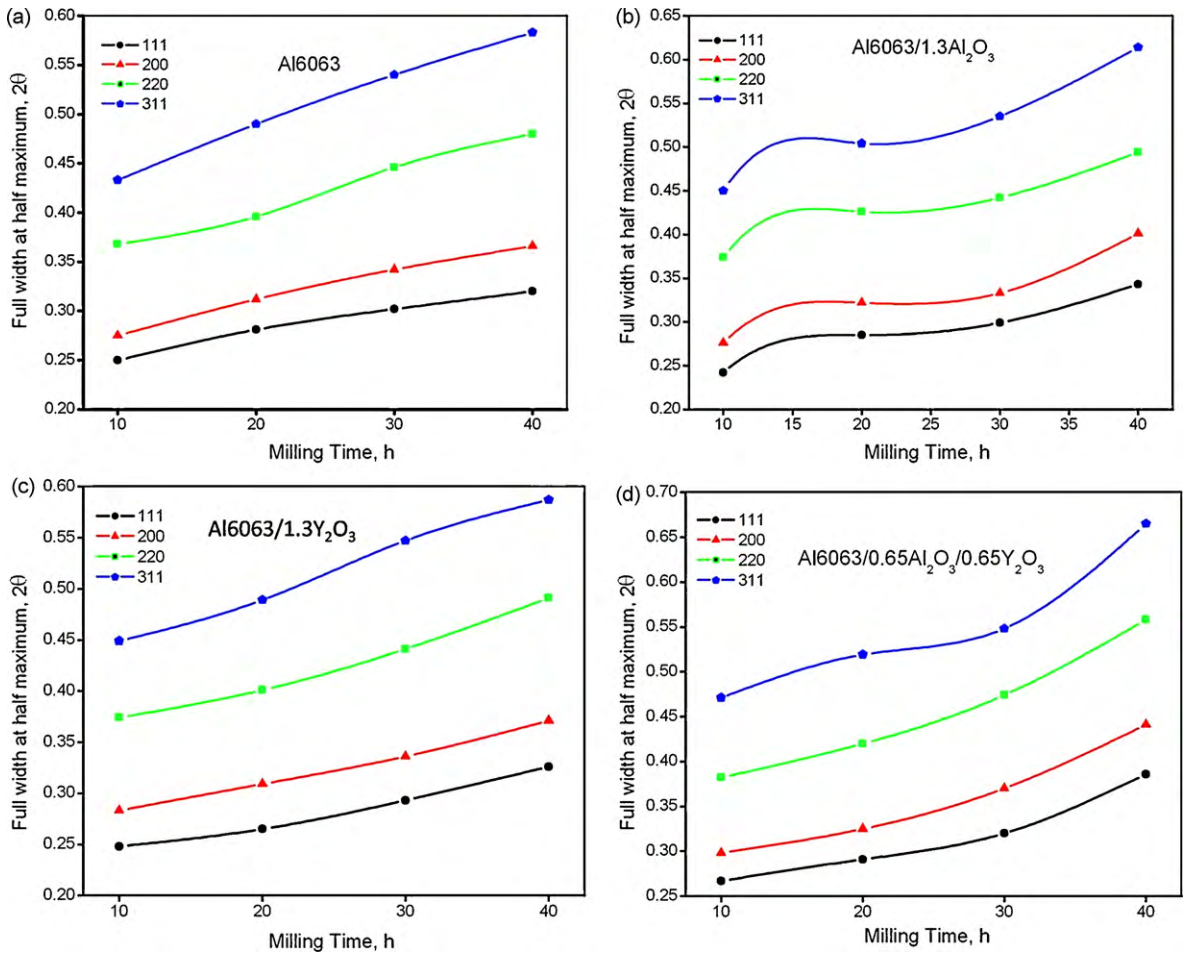


**Fig. 6.** Full width at half-maximum intensity of four diffraction planes as a function of milling time: (a) Al 6063 (b) Al 6063/1.3$Al_2O_3$ (c) Al 6063/1.3$Y_2O_3$ (d) Al 6063/0.65$Al_2O_3$/0.65$Y_2O_3$.

confirms the good interfacial integrity between soft aluminium matrix and nano reinforcement particles. The corresponding EDS spectrum shown as inset verifies the presence of nano particles.

### 3.2. *Effect of nano-size reinforcement on particle size distribution*

Fig. 3 shows the particle size distribution of Al 6063, Al 6063/1.3$Al_2O_3$, Al 6063/1.3$Y_2O_3$ and Al 6063/0.65$Al_2O_3$/0.65$Y_2O_3$ nano-composite powders milled for 40 h. Vertical columns refers to the average particle/agglomerate size (diameter). The high peak column represents the average particle/agglomerate size ($D_{50}$) and Table 2 presents $D_{50}$ and $D_{90} - D_{10}$ values related to the size distribution of above-mentioned powders. $D_{50}$ means average particle/agglomerate size equivalent to 50% of the particles and $D_{90} - D_{10}$ express the extension of size distribution.

After 40 h of milling the particle size distribution of Al 6063, as shown in Fig. 3(a), broadens as compared to the as-received powder and its average particle/agglomerate size increases to 30.51 μm. The broader particle size distribution is due to the predominance of particle deformation, while the increase in equivalent diameter size indicates the occurrence of welding between matrix particles. The particle size distribution is asymmetric with a deviation of the size distribution to the right indicates particles welding with themselves and other alloying matrix elements.

Fig. 3(b) shows the particle size distribution of Al 6063/1.3$Al_2O_3$ MA nano-composite powder milled for 40 h, indicating asymmetric and narrower size distribution. The skewed distribution of particles is because fracture consumes smaller range while welding consumes the larger range of particles [34]. Since alumina being the most stable oxide of aluminium, for a longer period of milling, it has a tendency either to react with the soft aluminium matrix by dissolution or can form a thin alumina layer at the interface. However, as no heat treatment was applied in this work, it was observed that, alumina particles have engaged and entrapped in the soft aluminium matrix mechanically. Hence larger range of particles consumes welding as evident from SEM micrograph shown in Fig. 2(e).

Fig. 3(c) shows the particle size distribution of Al 6063/1.3$Y_2O_3$ MA nano-composite powder after 40 h of milling. The above figure indicates a symmetric distribution, explaining the equilibrium between fracture and welding, typical form of the final stage of mechanical alloying/mechanical milling. The closer distribution is due to the occurrence of welding especially on the smaller particles and fracture on the higher particles [35].

Fig. 3(d) shows the particle size distribution of Al 6063/0.65$Al_2O_3$/0.65$Y_2O_3$ MA nano-composite powder milled for 40 h. Symmetric and broader distribution of particles indicates the occurrence of equilibrium between fracture and welding, typical of the final stage of mechanical alloying/mechanical milling. Hence, it is worth noting to say two interesting things (i) the reinforcement of spherical shaped hard nano-sized $Al_2O_3$ particles results in a significant decrease of average particle size, $D_{50}$, when compared with addition of the irregular shaped $Y_2O_3$ hard particles of equal volume fraction, and (ii) Al 6063/0.65$Al_2O_3$/0.65$Y_2O_3$

**Table 3**
Grain size of powders after 10, 20, 30 and 40 h of milling.

| Powder | Grain size in nm | | | |
|---|---|---|---|---|
| | Milled powder (h) | | | |
| | 10 | 20 | 30 | 40 |
| Al 6063 | 65.71 | 55.46 | 53.53 | 53.12 |
| Al 6063/1.3$Al_2O_3$ | 69.68 | 49.7 | 48.99 | 41.51 |
| Al 6063/1.3$Y_2O_3$ | 63.31 | 61.08 | 51.93 | 42.53 |
| Al 6063/.65$Al_2O_3$/.65$Y_2O_3$ | 55.24 | 48.14 | 42.79 | 36.68 |

**Table 4**
Lattice strain of powders after 10, 20, 30 and 40 h of milling.

| Powder | Lattice strain in % | | | |
|---|---|---|---|---|
| | Milled powder (h) | | | |
| | 10 | 20 | 30 | 40 |
| Al 6063 | 0.15 | 0.16 | 0.19 | 0.21 |
| Al 6063/1.3$Al_2O_3$ | 0.15 | 0.15 | 0.16 | 0.19 |
| Al 6063/1.3$Y_2O_3$ | 0.15 | 0.17 | 0.17 | 0.17 |
| Al 6063/.65$Al_2O_3$/.65$Y_2O_3$ | 0.15 | 0.15 | 0.16 | 0.19 |

powder mixture results in a hardly unchanged average particle/agglomerate size in relation with Al 6063/0.65$Al_2O_3$ powder mixture, and provides uniform particle size distribution when compared with individual hard ceramic reinforcement particles. The fracturing tendency was due to combination of more collision with balls and more support from hard ceramic particles. This is evident from earlier discussions of correlation between particle size and phenomenon of various welding and fracture mechanism in the high-energy milling process. XRD patterns shown in Fig. 4(a) and (b), discussed in subsequent Section 3.4, also confirm that no inter-metallic compound was formed at the Al/1.3$Al_2O_3$ or Al/1.3$Y_2O_3$ interface.

### 3.3. EDAX analysis

Fig. 4(a) and (b) shows the EDAX spectra for the Al 6063 and Al 6063/0.65$Al_2O_3$/0.65$Y_2O_3$ nano-composite powder mixture, respectively. The presence of only Al and O as noticed from the peaks present in the spectrum, confirms that the milled powder did not contain any additional element due to contamination from the milling media such as grinding vessel and balls. The absence

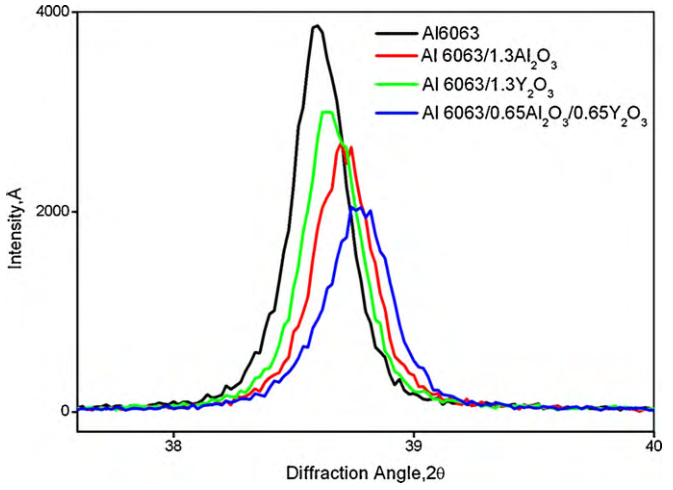


**Fig. 7.** XRD patterns of first peak from the diffracting plane (1 1 1) for: Al 6063, Al 6063/1.3$Al_2O_3$, Al 6063/1.3$Y_2O_3$, Al 6063/0.65$Al_2O_3$/0.65$Y_2O_3$ nano-composite powder after 40 h of milling, showing the sharp diffraction peaks of Al getting broadened and reduced in intensity.

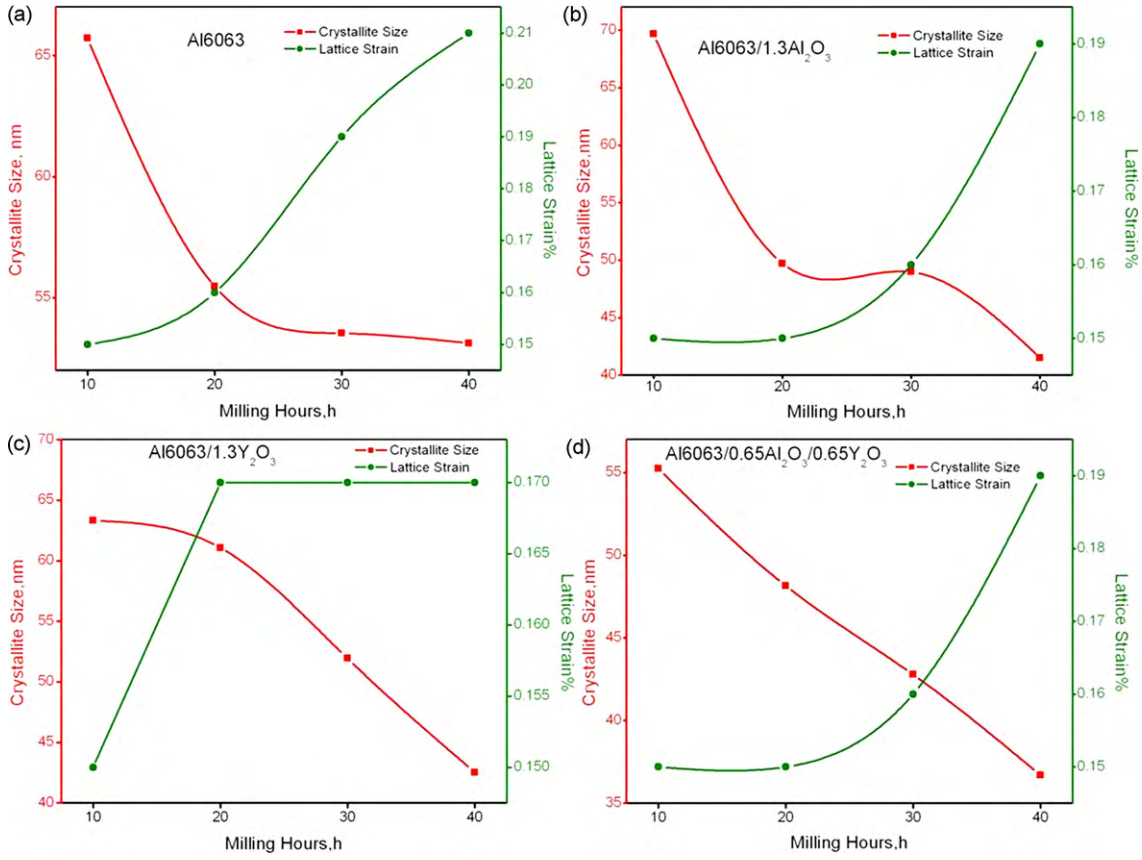


**Fig. 8.** Variation in crystallite size and lattice strain as a function of milling time: (a) Al 6063 (b) Al 6063/1.3$Al_2O_3$ (c) Al 6063/1.3$Y_2O_3$ (d) Al 6063/0.65$Al_2O_3$/0.65$Y_2O_3$.

of clear peaks from any other element indicates that no significant contamination of the milled powders has occurred. It may also be noted that even though only Al and O peaks are seen in the two patterns, the intensity of the O peak is increasing with increasing nano-sized reinforcement, as expected from the increased amount of oxygen in the powder mixture containing volume fraction of nano-sized $Al_2O_3/Y_2O_3$.

### 3.4. X-ray diffraction analysis

The X-ray diffraction patterns of Al 6063, Al 6063/1.3$Al_2O_3$, Al 6063/1.3$Y_2O_3$, Al 6063/0.65$Al_2O_3$/0.65$Y_2O_3$ powders milled after 10, 20, 30 and 40 h of milling are shown in Fig. 5. The diffraction patterns of the nano-crystalline powder exhibited various peaks corresponding to the face centered cubic (FCC) phase of Al. Al peaks, $Al_2O_3$ peaks and $Y_2O_3$ peaks were indexed using JCPDS file numbers 04-0787, 86-1410 and 86-1107, respectively. The absence of other peaks of the alloying matrix elements can be attributed to the limitation of the filtered X-ray to detect phases with amount less than 2% volume fraction [32].

Noticeable shift in the position (i.e., 2$\theta$ angles) of the Al peaks was observed in Fig. 5(a)–(d) with the increase of milling time. Enlarged view of shift in the position (i.e., 2$\theta$ angles) of the Al (1 1 1) and Al (2 0 0) peaks is shown in the inset of Fig. 5(a)–(d). The shift was measurable and this could be related to the dissolution of atoms related to minor matrix alloying elements and reinforcement particles in the lattice of aluminium during high-energy ball milling. This suggests the formation of Al-based solid solutions and an increase in the solute concentration as the milling time increases. Similar observation was made by the earlier researchers in their work [11,21]. The other matrix alloying elements were crushed, nano-crystallized and finally amorphosized, as evidenced through HRTEM image (Fig. 10).

X-ray diffraction line broadening (expressed as full width at the half-maximum intensity) with milling time for all the Al 6063 blended systems was presented in Fig. 6. As the milling time increases, significant reduction in peak height and broadening of the same was observed as explained by the earlier researchers [4,29] and this may be ascribed to a severe lattice distortion and grain size refinement. The change in crystallite size and lattice strain of powders milled for 40 h was calculated using Williamson and Hall Eq. (2) and the results are given in Tables 3 and 4, respectively. Fig. 7 shows the XRD patterns for first peak of the Al diffracting plane (1 1 1), for pure Al 6063 and different composite

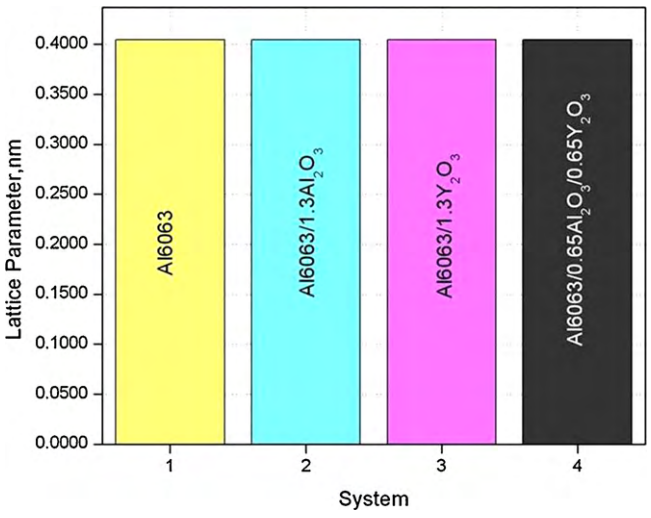


**Fig. 9.** Variation in lattice parameter as a function milling time for powders milled for 40 h.

powders milled for 40 h, which interprets that the peak lines which are stronger and narrower has larger crystallite size and reduced lattice strain.

The effects of milling time on the grain size and the lattice strain for Al 6063 powder mixtures are shown in Fig. 8. The most intensive grain refinement and the strongest increase of the lattice strain occur in the early stage of milling and up to 20 h. In the period from 20 to 40 h of the milling time, the grain size of Al 6063 (Fig. 8(a)) remains almost constant due to rise in surface and strain energy of the particles. Grain refinement of Al 6063/1.3$Al_2O_3$, Al 6063/1.3$Y_2O_3$, Al 6063/0.65$Al_2O_3$/0.65$Y_2O_3$ powder mixture (Figs. 8(b)–(d)) was still continued due to the presence of hard ceramic particles and lattice distortion. At milling time longer than 20 h, the lattice strain remains constant in case of Al 6063/1.3$Y_2O_3$ powder (Fig. 8(c)). In general, the lattice strain curve gradually increases and attains maximum value which is ascribed to the grain size reduction and its effect on strain reduction. Higher grain size refinement and lattice strain changes are more pronounced in Al 6063/0.65$Al_2O_3$/0.65$Y_2O_3$ MA nano-composite powder (Fig. 8(d)).

The lattice parameter was calculated for each of the Al diffracting planes, from the XRD patterns as explained by Cullity [32]. Fig. 9 shows the variation of lattice parameter for different powders with

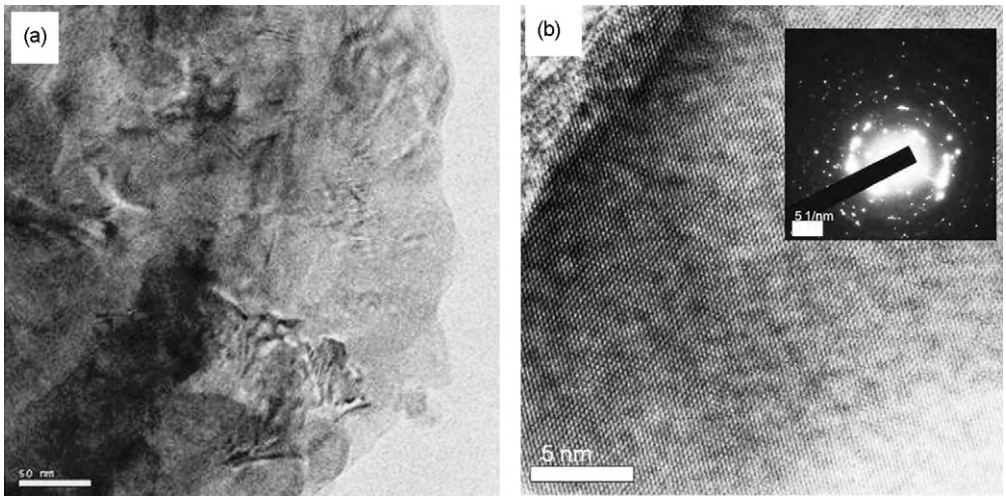


**Fig. 10.** HRTEM image of mechanically alloyed Al 6063/0.65$Al_2O_3$/0.65$Y_2O_3$ nano-composite powders (a) showing no inter-metallic compound/layer formed between Al matrix and nano particles (b) showing lattice fringes after 40 h of milling. Inset is the selected area diffraction pattern from the sample.

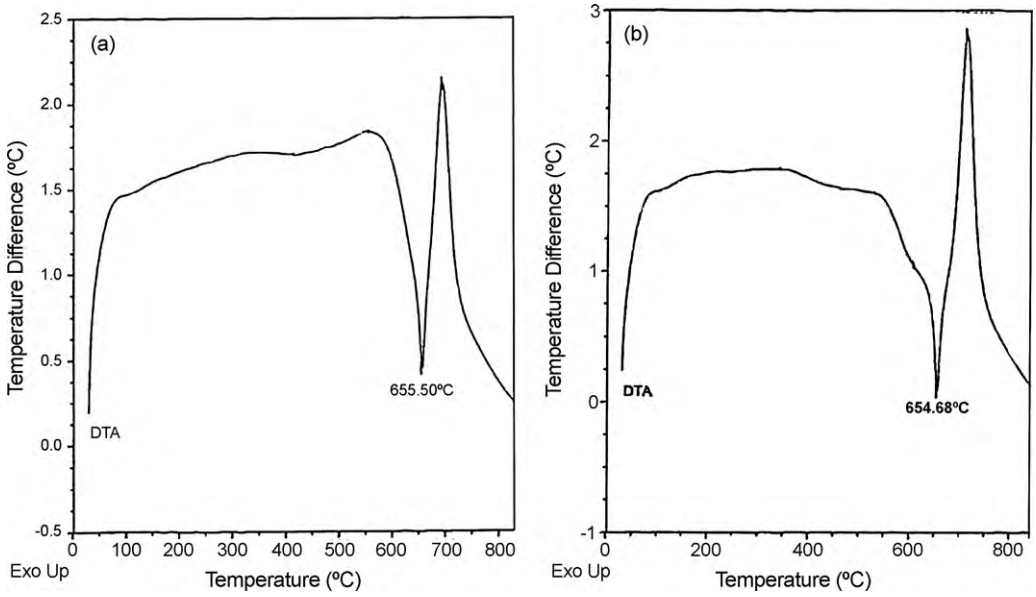


**Fig. 11.** The DTA curve of (a) Al 6063 and (b) Al 6063/0.65$Al_2O_3$/0.65$Y_2O_3$ composite powders by mechanical alloying after 40 h.

respect to milling time. All the powders investigated have almost equal amount of low shift in lattice parameter. The reinforcement particles embedded in Al lattice are clearly seen in Fig. 2(e), (g) and (h) indicating a reduction in lattice parameter. It is noticed that the lattice parameter decreases with increasing milling time, suggesting the formation of Al-based solid solutions. The observed decrease in the lattice parameter is consistent with the possible formation of Al solid solutions with Fe, Cr, Cu, Mg, Ti, Si, Zn, Mn, Y and O element from alumina and yttria solutes. The dissolution of Fe, Cr, Cu, Mg, Ti, Si, Zn, Mn, Y and O elements into Al will decrease the lattice parameter of Al, because the atomic sizes of Fe, Cr, Cu, Si, Zn, Mn, Y and O elements are smaller than that of Al, whereas the atomic size of Ti and Mg is similar to that of Al [36].

Fig. 10(a) shows HRTEM dark field image of mechanically alloyed Al 6063/0.65$Al_2O_3$/0.65$Y_2O_3$ nano-composite powder which confirms that no inter-metallic compound/layer was formed at the interface of aluminium matrix and reinforcement. Fig. 10(b) shows HRTEM image of mechanically alloyed Al 6063/0.65$Al_2O_3$/0.65$Y_2O_3$ nano-composite powder showing lattice fringes after 40 h of high-energy wet ball milling. The inset in the figure represents the selected area diffraction pattern with continuous rings, which confirms the nano-crystalline nature of the composite powder. The bright areas in the micrograph correspond to nano-sized reinforcement crystallites. The crystallite size calculated from X-ray peak broadening and absence of other peaks indicating no formation of inter-metallic layer are in close agreement with that of HRTEM observations.

DTA analysis was conducted to study the powder displacement reactions in the milled powder. The addition of reinforcement particles in the aluminium matrix does not alter much in the nature of exothermic peaks observed in the pure Al 6063 alloy powder. The broad exothermic peak from 100 to 557.20 °C (Fig. 11(a)) in Al 6063 powder mixture, from 100 to 533.57 °C (Fig. 11(b)) in Al 6063/0.65$Al_2O_3$/0.65$Y_2O_3$ powder mixture occurred over the period of time attributes to strain release and grain growth [37,38]. The endothermic peak at 655.60 °C (Fig. 11(a)) in Al 6063 powder mixture and the endothermic peak at 654.80 °C (Fig. 11(b)) in Al 6063/0.65$Al_2O_3$/0.65$Y_2O_3$ powder mixture correspond to the melting of aluminium. Also, it can be observed that after the melting point of aluminium a steady solid exothermic reaction occurs between the matrix powder and the reinforcement particles.

## 4. Conclusions

The morphological and structural changes of aluminium powder milled for 40 h reinforced with nanometric ceramic particles were studied. In the present study, comparisons of individual and combined reinforcement of alumina and yttria nano ceramic particles are realized.

1. Addition of ceramic nano particles into the aluminium matrix sustains the crystallite size reduction. When compared to the aluminium alloy composite reinforced with alumina or yttria nano particles, the composite powder reinforced with both alumina and yttria results in much better reduction in crystallite size, which is due to the increase in fracture tendency.
2. High-energy wet ball milling method used for the preparation of nano-composite powders with nano particles reinforcement, resulted in refined microstructure and randomly oriented interfacial grain boundaries which is the characteristic of particles at steady-state condition.
3. Better particle size distribution was attained in Al 6063/$Al_2O_3$/$Y_2O_3$ nano-composite powder, as distinguished from individual reinforcements due to the balance between welding and fracture which confirms the attainment of steady-state condition.

## Acknowledgements

The authors thank the Institute for the project grant to carry out the investigation. The facilities made available under DST project (SR/FTP/ETA-69/07), Government of India, are gratefully acknowledged.

## References

[1] D.B. Miracle, Compos. Sci. Technol. 65 (2005) 2526–2540.
[2] J.M. Torralba, C.E. da Costa, F. Velasco, J. Mater. Process. Technol. 133 (2003) 203–206.
[3] E.M. Ruiz-Navas, J.B. Fogagnolo, F. Velasco, J.M. Ruiz_Prieto, L. Froyen, Composites Part A 37 (2006) 2114–2120.
[4] C. Suryanarayana, Prog. Mater. Sci. 46 (2001) 1–184.
[5] J.B. Fogagnolo, F. Velasco, M.H. Robert b, J.M. Torralba, Mater. Sci. Eng. A 342 (2003) 131–143.
[6] L. Shaw, H. Luo, J. Villegas, D. Miracle, Scripta Mater. 50 (2004) 921–925.

[7] Y.Q. Liu, H.T. Cong, W. Wang, C.H. Sun, H.M. Cheng, Mater. Sci. Eng. A 505 (2009) 151–156.
[8] Y.S. Park, K.H. Chung, N.J. Kim, E.J. Lavernia, Mater. Sci. Eng. A 374 (2004) 211–216.
[9] Z.H. Zhang, B.Q. Han, D. Witkin, L. Ajdelsztajn, E.J. Laverna, Scripta Mater. 54 (2006) 869–874.
[10] M.J. Hadianfard, J. Healy, Y.W. Mai, J. Mater. Sci. 29 (1994) 2321–2327.
[11] B. Prabhu, C. Suryanarayana, L. An, R. Vaidyanathan, Mater. Sci. Eng. A 425 (2006) 192–200.
[12] M. Sherif El-Eskandarany, J. Alloys Compd. 279 (1998) 263–271.
[13] Ismail Ozdemir, Sascha Ahrens, Silke Mucklich, Bernhard Wielage, J. Mater. Process. Technol. 205 (2008) 111–118.
[14] S.M. Zebarjad, S.A. Sajjadi, Mater. Des. 27 (2006) 684–688.
[15] M. Khakbiz, F. Akhlaghi, J. Alloys Compd. 479 (2009) 334–341.
[16] Y. Saberi, S.M. Zebarjad, G.H. Akbari, J. Alloys Compd. 484 (2009) 637–640.
[17] I. Estrada-Guel, C. Carreno-Gallardo, D.C. Mendoza-Ruiz, M. Miki_Yoshida, E. Rocha-Rangel, R. Martinez-Sanchez, J. Alloys Compd. 483 (2009) 173–177.
[18] R. Perez-Bustamante, C.D. Gomez-Esparza, I. Estrada-Guel, M. Miki-Yoshida, L. Licea-Jimenez, S.A. Pérez-García, R. Martínez-Sanchez, Mater. Sci. Eng. A 502 (2009) 159–163.
[19] Hamid Abdoli, Hamed Asgharzadeh, Ismail Salahi, J. Alloys Compd. 473 (2009) 116–122.
[20] S.S. Nayak, S.K. Pabi, B.S. Murty, J. Alloys Compd. 492 (2010) 128–133.
[21] S. Sivasankaran, K. Sivaprasad, R. Narayanasamy, Vijay Kumar Iyer, J. Alloys Compd. 491 (2010) 712–721.
[22] R.J. Arsenault, Mater. Sci. Eng. 64 (2) (1984) 171–181.
[23] A. Mazaherya, H. Abdizadeha, H.R. Baharvandi, Mater. Sci. Eng. A 518 (2009) 61–64.
[24] K.S. Tun, M. Gupta, J. Alloys Compd. 487 (2009) 76–82.
[25] S.F. Hassan, M. Gupta, Mater. Sci. Eng. A 392 (2005) 163–168.
[26] W.L.E. Wong, M. Gupta, Compos. Sci. Technol. 67 (2007) 1541–1552.
[27] S.F. Hassan, M. Gupta, J. Mater. Sci. 41 (2006) 2229–2236.
[28] C. Suryanarayana, E. Ivanov, V.V. Boldyrev, Mater. Sci. Eng. A 304–306 (2001) 151–158.
[29] Viseslava Rajkovic, Dusan Bozic, Milan T. Jovanovic, J. Alloys Compd. 459 (2008) 177–184.
[30] C.S. Goh, J. Wei, L.C. Lee, M. Gupta, Acta Mater. 55 (2007) 5115–5121.
[31] K. Williamson, W.H. Hall, Acta Metall. 1 (1953) 22–31.
[32] B.D. Cullity, Elements of X-ray Diffraction, third ed., Prentice Hall, London, 2001.
[33] Z. Razavi-Hesabi, A. Simchi, S.M. Seyed Reihani, Mater. Sci. Eng. A 428 (2006) 159–168.
[34] S.S. Razavi Tousi, R. Yazdani Rad, E. Salahi, I. Mobasherpour, M. Razavi, Powder Technol. 192 (2009) 346–351.
[35] J. Lee, S. Kim, C. Park, C. Bae, J. Mater. Process. Manuf. Sci. 4 (1995) 55.
[36] P. Haasen, Physical Metallurgy, third ed., Cambridge University Press, Cambridge,Great Britain, 1996.
[37] Maryam Azabou, Mohamed Khitouni, Abdelwaheb Kolsi, Mater. Charact. 60 (2009) 499–505.
[38] R. Maiti, M. Chakraborty, J. Alloys Compd. 458 (2008) 450–456.